Identification and molecular analysis of *RNF31* Q622H germline polymorphism

SESHIRU NAKAZAWA[1], RYO MAMIYA[1], REIKA KAWABATA-IWAKAWA[2], DAISUKE OIKAWA[3], KYOICHI KAIRA[4], FUMINORI TOKUNAGA[3], SUMIHITO NOBUSAWA[5], YUSUKE SATO[6], ATSUSHI SASAKI[7], TOSHIKI YAJIMA[8] and KEN SHIRABE[1]

[1]Department of General Surgical Science, Gunma University Graduate School of Medicine; [2]Division of Integrated Oncology Research, Gunma University, Initiative for Advanced Research, Maebashi, Gunma 371-8511; [3]Department of Medical Biochemistry, Graduate School of Medicine, Osaka Metropolitan University, Osaka, Osaka 545-8585; [4]Department of Respiratory Medicine, Comprehensive Cancer Center, International Medical Center, Saitama Medical University, Hidaka, Saitama 350-1298; [5]Department of Human Pathology, Gunma University Graduate School of Medicine, Maebashi, Gunma 371-8511; [6]Center for Research on Green Sustainable Chemistry, Tottori University, Tottori, Tottori 680-8552; [7]Department of Pathology, Saitama Medical University School of Medicine, Moroyama, Saitama 350-0495; [8]Department of Innovative Cancer Immunotherapy, Gunma University Graduate School of Medicine, Maebashi, Gunma 371-8511, Japan

Received April 21, 2022; Accepted August 1, 2022

DOI: 10.3892/ol.2022.13514

Abstract. The linear ubiquitin chain assembly complex (LUBAC), which is composed of RING finger protein 31 (RNF31), RANBP2-type and C3HC4-type zinc finger containing 1 and SHANK-associated RH domain interactor subunits, is the only ubiquitin ligase to generate Met1-linked linear ubiquitin chains. Linear ubiquitin chains regulate canonical NF-κB activation and cell death. Single nucleotide polymorphisms in *RNF31*, such as Q584H and Q622L, are known to cause the activated B cell-like subtype of diffuse large B cell lymphoma (ABC-DLBCL) because of enhanced LUBAC-mediated NF-κB activation. The present study identified a novel Q622H polymorphism of *RNF31* in two patients with lung cancer, one of whom had concurrent ABC-DLBCL. Immunohistochemical analyses revealed that although the expression of RNF31 was elevated in both patients, only the ABC-DLBCL specimen showed increased NF-κB activation. Cancer panel analysis showed that the Q622H-related ABC-DLBCL did not harbor co-mutations that were previously reported in Q584H-/Q622L-related ABC-DLBCL. Furthermore, in contrast to Q584H and Q622L, Q622H showed no enhancement effects on LUBAC and NF-κB activity *in vitro* compared with wild-type RNF31. The present study's structural prediction suggested that the electrostatic interaction related to the Q622 residue may not have had an important role in LUBAC formation. In conclusion, the molecular mechanism and mutational background of *RNF31* Q622H differed from that of *RNF31* Q584H or Q622L. Furthermore, *RNF31* Q622H appeared not to induce NF-κB activation in lung cancer.

Correspondence to: Dr Seshiru Nakazawa, Department of General Surgical Science, Gunma University Graduate School of Medicine, 3-39-22 Showa-machi, Maebashi, Gunma 371-8511, Japan
E-mail: snakazawa@gunma-u.ac.jp

Key words: lung cancer, B-cell lymphoma, RING finger protein 31, NF-κB, linear ubiquitin

Introduction

The ubiquitin system, which is composed of ubiquitin-activating enzyme, ubiquitin-conjugating enzyme, and ubiquitin ligase, regulates numerous cellular functions including proteasomal degradation and signal transduction through the generation of various ubiquitin chains (1-3). Thus, dysfunctions in the ubiquitin system are associated with multiple disorders (4). The linear ubiquitin chain assembly complex (LUBAC), composed of RNF31 (also known as HOIP), RBCK1 (HOIL-1L), and SHARPIN subunits, specifically generates N-terminal M1-linked linear polyubiquitin chains (M1-Ub), which activate the nuclear factor-kappa B (NF-κB) pathway, affecting the development and activation of T cells and B cells (5-8). Accordingly, dysregulation of M1-Ub causes lymphoma (9-12), and two germline polymorphisms of RNF31, Q584H and Q622L, are specifically enriched in patients with activated B-cell-like subtype of diffuse large B-cell lymphoma (ABC-DLBCL) (10). These polymorphisms were reported to strengthen the interaction between RNF31 and RBCK1, subsequently increasing the ligase activity of LUBAC and NF-κB activation and causing ABC-DLBCL (10).

Because the role of dysregulated M1-Ub in other tumors is unclear, we first aimed to clarify the prevalence of *RNF31* Q584

and Q622 polymorphisms in patients with lung cancer. We identified two patients with a novel Q622H polymorphism. Interestingly, one patient also had a history of ABC-DLBCL. We thus speculated that the presence of ABC-DLBCL in the patient with *RNF31* Q622H polymorphism was not a coincidence and that the Q622H may have molecular functions similar to Q584H and Q622L. We further evaluated NF-κB activation and the mutational background in lung cancer and ABC-DLBCL with *RNF31* Q622H polymorphism, and analyzed the molecular effects of *RNF31* Q622H on LUBAC activation.

Materials and methods

Patients and clinical course. We analyzed *RNF31* polymorphisms in exon 10 of *RNF31* in lung cancer patients who underwent surgery in our department from 2003 to 2019. Details of the clinical courses of patients with the *RNF31* Q622H polymorphism are described in the Results section.

PCR amplification and sanger sequencing. The primers used to amplify *RNF31* exon 10 were as follows: forward 5'-CTG GGCTGGGTGCCTTTTCCTGTCAGG-3' and reverse 5'-GAGTAATTCTTGGACCAGGTATCG-3' (10). The PCR products were purified using the ExoSAP-IT Kit (Thermo Fisher Scientific) and sequenced using the BigDye sequencing system (Applied Biosystems).

Immunostaining. Immunohistochemistry was performed on four-micrometer-thick formalin-fixed [10% neutral buffered formalin for 24 to 48 h at room temperature (RT)], paraffin-embedded (FFPE) tissue sections as previously described (13,14). For RNF31 immunostaining (Fig. S1), deparaffinized and rehydrated sections were treated with 0.3% hydrogen peroxide (H_2O_2) in methanol for 30 min at RT to block endogenous peroxidase activity. Antigen retrieval was performed by autoclaving (5 min, citrate buffer pH 6.0). The sections were incubated with anti-RNF31/HOIP antibody (ab187976; Abcam; 1:50 dilution) overnight at 4˚C, followed by incubation with a Histofine Simple Stain MAX PO (Nichirei), for 45 min at RT. The peroxidase reaction was carried out using 0.02% 3,3'-diaminobenzidine tetrahydrochloride and 0.01% H_2O_2 in 0.05 M Tris-HCl (pH 7.4). The immunoreaction was visualized with diaminobenzidine (DAB) and briefly counterstained with hematoxylin. Negative control tissue sections were stained as described above, except that the primary antibody was omitted. For p65 immunostaining, antigen retrieval was performed by autoclaving (10 min, citrate buffer pH 6.0). The sections were incubated with anti-NF-κB p65 antibody (D14E12, Cell Signaling Technology; 1:400 dilution), overnight at 4˚C, followed by immersing the sections in 3% solution of H_2O_2 for 10 min at RT to block endogenous peroxidase activity. Next, addition of a Histofine Simple Stain MAX PO (Nichirei) was carried out for 30 min at RT. The immunoreaction was visualized with DAB and briefly counterstained with hematoxylin for 30 to 60 sec. Nuclear staining of NF-κB p65 was rated positive.

Genomic DNA extraction. DNA from fresh frozen lung cancer tissue and adjacent normal lung tissue were extracted using a DNeasy Tissue Kit (QIAGEN). DNA from peripheral blood mononuclear cells was extracted using a QIAamp DNA Blood Mini Kit (QIAGEN) and that from ABC-DLBCL FFPE tissue was extracted from four micro-dissected slides using a GeneRead DNA FFPE Kit (QIAGEN), all in accordance with the manufacturer's instructions.

Genetic analysis. QIAseq DNA QuantiMIZE Kit (QIAGEN) was used to qualify and quantify amplifiable FFPE DNA prior to the library preparation. Ten nanograms (fresh frozen samples) or 100 ng (FFPE samples) genomic DNA were subjected to genetic analysis using the Human Comprehensive Cancer QIAseq DNA Panel (QIAGEN). For each library, DNA concentrations and fragment sizes were measured using the Qubit dsDNA HS Assay Kit (Thermo Fisher Scientific) and the Bioanalyzer High Sensitivity DNA Kit (Agilent), respectively. Paired-end sequencing was performed on a NextSeq 500 platform (Illumina) for 151x2 cycles. The average number of read fragments was 22,444,402 (range 17,939,522-30,178,462). Read fragments were aligned to the hg19 assembly of the human genome (Genome Reference Consortium Human Build 37, GRCh37) and variants were called using the GeneGlobe v.2 smCounter (QIAGEN). The average coverage depth and the percentage of target coverage at ≥20x were 3,573.19 (range 3,025.23-4,366.68) and 98.68% (range, 98.18%-99.03%), respectively. VCFtools (v. 0.1.17) was used to filter out all variants other than 'Pass' variants with following command: 'vcf-annotate-hard-filter'. Variants were annotated using the ANNOVAR (http://annovar.openbioinformatics.org/en/latest/) pipeline. Affectable mutation candidates were those with: 1) amino acid changes or variants on splice site; 2) low minor allele frequency in Japanese and east Asian populations (<0.01, HGVD2, DBexome20161214; https://www.hgvd.genome.med.kyoto-u.ac.jp, gnomAD exome EAS, v. 2.0.1); and 3) variant allele frequency >0.05. In total, 15 variants were detected in at least one sample. Furthermore, five variants with COSMIC v.70 (15) (cancer.sanger.ac.uk) registration were selected.

Cell culture, transfection, and luciferase assay. *RNF31*-knockout (KO) 293T cells were cultured in DMEM containing 10% fetal bovine serum, 100 IU/ml penicillin G, and 100 μg/ml streptomycin at 37˚C under 5% CO_2. Transfection experiments were performed using polyethyleneimine (PEI MAX; Polysciences). Briefly, plasmid DNA and PEI [1:2 ratio of total DNA (μg): PEI (μg)] were mixed in PBS, and incubated for 15 min at RT. Then the DNA/PEI mixture was added to cells. For the luciferase assay, a pGL4.32 [luc2P/NF-κB-RE/Hygro] vector and a pRL-TK *Renilla* Luciferase control reporter vector (Promega) were co-transfected into *RNF31*-KO 293T cells with a FLAG-RNF31 expression vector (wild-type or mutant), RBCK1-myc, and HA-SHARPIN. At 24 h after transfection, the cells were lysed, and the luciferase activity was measured using a GloMax 20/20 luminometer (Promega) using the Dual-Luciferase Reporter Assay System (Promega). The enzyme activity of Renilla luciferase was used to normalize the firefly luciferase enzyme activity.

Construction of RNF31-KO cells. A gRNA cloning vector and a pCAG-hCas9 vector were obtained from Addgene. The nucleotide sequence 5'-TCAACCCTCAGGAAGCTCAGC-3' in exon 2 of human *RNF31* was selected as the target. These plasmids and a puromycin-resistant vector (pXS-Puro) were co-transfected into 293T cells (ATCC), and puromycin-resistant cell clones were selected by limiting dilution. Genome editing of *RNF31* was screened by a *BtsCI* digestion assay (New England BioLabs), and mutations were confirmed by sequencing. RNF31 protein deficiency was confirmed by immunoblotting (Fig. S2).

Immunoprecipitation, SDS-PAGE, and immunoblotting. FLAG-RNF31, RBCK1-myc, and HA-SHARPIN plasmids were co-transfected into *RNF31*-KO 293T cells. At 24 h after transfection, the cells were lysed with 50 mM Tris-HCl, pH 7.5, 150 mM NaCl, 1% Triton X-100, 2 mM PMSF, and complete protease inhibitor cocktail (Sigma). The Bradford protein assay was performed to determine the protein concentration. For immunoprecipitation, 800 μg of the cell lysates was incubated with 1 μg of anti-FLAG antibody (F7425; Sigma-Aldrich) or normal rabbit IgG (PM035; MBL) for 1 h at 4˚C, and centrifuged at 20,000 g for 10 min at 4˚C. The supernatants were incubated with Protein G agarose beads (30 μl of the 50% slurry; GE Healthcare) for 1 h at 4˚C with gentle rotation. Then, beads were washed three times with 1 ml of lysis solution, centrifuged at 1,500 g for 4 min at 4˚C. The samples were heated at 95˚C for 5 min with SDS-PAGE sample buffer, and separated by SDS-PAGE and transferred to PVDF membranes. For SDS-PAGE, 2/15% gradient gel (Cosmobio) or 7.5% gel was used and transferred to PVDF membranes. After blocking the membrane in Tris-buffered saline containing 0.1% Tween-20 (TBS-T) with 5% skim-milk for 2 h at RT, the membrane was incubated with the appropriate primary antibodies diluted in TBS-T containing 5% skim-milk at 4˚C overnight. Then, the membranes were incubated with anti-mouse IgG horseradish peroxidase-conjugated secondary antibody (NA931V; 1:10,000; Cytiva) or anti-rat IgG horseradish peroxidase-conjugated secondary antibody (NA935; 1:10,000; Cytiva) diluted in TBS-T containing 5% skim-milk for 2 h at RT when using non-HRP-conjugated primary antibodies. For detection, SuperSignal West Pico PLUS (34577; Thermo Fisher Scientific) or Luminata Forte (WBLUF0100; Millipore) was used.

Plasmids. The human cDNA open reading frame of RNF31 (16,17) was amplified by reverse transcription PCR. Mutants of this cDNA was prepared by the QuikChange method, and all nucleotide sequences were verified. The cDNAs were ligated to the appropriate epitope sequences and cloned into the pcDNA3.1 vector (Invitrogen).

Antibodies. The following antibodies were used for immunoblotting analyses: DYKDDDDK (1E6, 015-22391; HRP-conjugate; 1:20,000; Wako), tubulin (CLT9002; 1:3,000; Cedarlane), β-actin (sc-47778, 1:250; Santa Cruz Biotechnology), Myc (HRP-Conjugate, M192-7; 1:20,000; MBL), HA (HRP-Conjugate, M180-7; 1:20,000; MBL), HA (11867423001; 1:1,000; Roche), and linear ubiquitin (clone LUB9, MABS451; 1:1,000; Millipore), RNF31/HOIP (ab125189; 1:1,000; Abcam), RBCK1 (sc-49718, 1:250; Santa Cruz Biotechnology), SHARPIN (14626-1-AP; 1:3,000; Proteintech).

Statistics. Data are shown as means ± SEM from at least three experiments performed in triplicate. One-way ANOVA followed by a post hoc Tukey HSD test or Student's t-test was performed using KaleidaGraph software (Synergy Software, PA, USA). For all tests, a P-value of less than 0.05 was considered statistically significant.

Results

Analysis of RNF31 polymorphisms in lung cancer patients. To identify the *RNF31* Q584 and Q622 polymorphisms, we sequenced exon 10 of *RNF31* in 481 patients with lung adenocarcinoma, 152 with squamous cell carcinoma, 16 with large cell neuroendocrine carcinoma, 2 with adenosquamous carcinoma, and 22 with small cell lung cancer (Table SI). Although the reported prevalence of Q584H and Q622L polymorphisms in healthy individuals is 0.95% (GO Exome Sequencing Project and 1000 Genome Project), no patient harbored these polymorphisms in our cohort. However, two patients had a Q622H polymorphism (Fig. 1A), which was not identified in public databases (SNPnexus: https://www.snp-nexus.org/v4/). More interestingly, one of these patients also had a history of ABC-DLBCL.

Clinical course of patients with RNF31 Q622H polymorphism. The first case was a 71-year-old Japanese patient who had undergone resection of lung adenocarcinoma, stage IB. The patient received postoperative oral chemotherapy for 2 years and had no recurrence at 5 years (Fig. 1B). The second case was a 78-year-old Japanese patient with a history of ABC-DLBCL (Fig. 1B). The patient underwent six cycles of R-CHOP therapy with radiation. One year later, the patient was diagnosed with lung cancer and underwent surgical resection. Pathological diagnosis was lung adenocarcinoma, stage IA. Two years later, the patient developed multiple lymph node metastases. The patient was administered vinorelbine but further developed malignant pleuritis. The patient then had pemetrexed as second-line, docetaxel as third-line, vinorelbine rechallenge as fourth-line, and tegafur/gimeracil/oteracil (TS-1) as fifth-line treatment. However, the disease progressed, and the patient eventually died of respiratory failure.

Histological analysis of lung cancer, recurrent lymph nodes, and ABC-DLBCL. The previously reported *RNF31* Q584H/Q622L polymorphisms strengthen RNF31-RBCK1 binding, which subsequently increase M1-Ub formation and NF-κB activation (10). We therefore analyzed whether the *RNF31* Q622H polymorphism had similar effects. Immunohistochemistry showed that both patients strongly expressed RNF31 in tumor tissues compared with the adjacent lung tissue (Fig. 2). NF-κB activation, evaluated by nuclear localization of p65, was only observed in the ABC-DLBCL specimen, and not in the lung cancer or recurrent lymph node specimens.

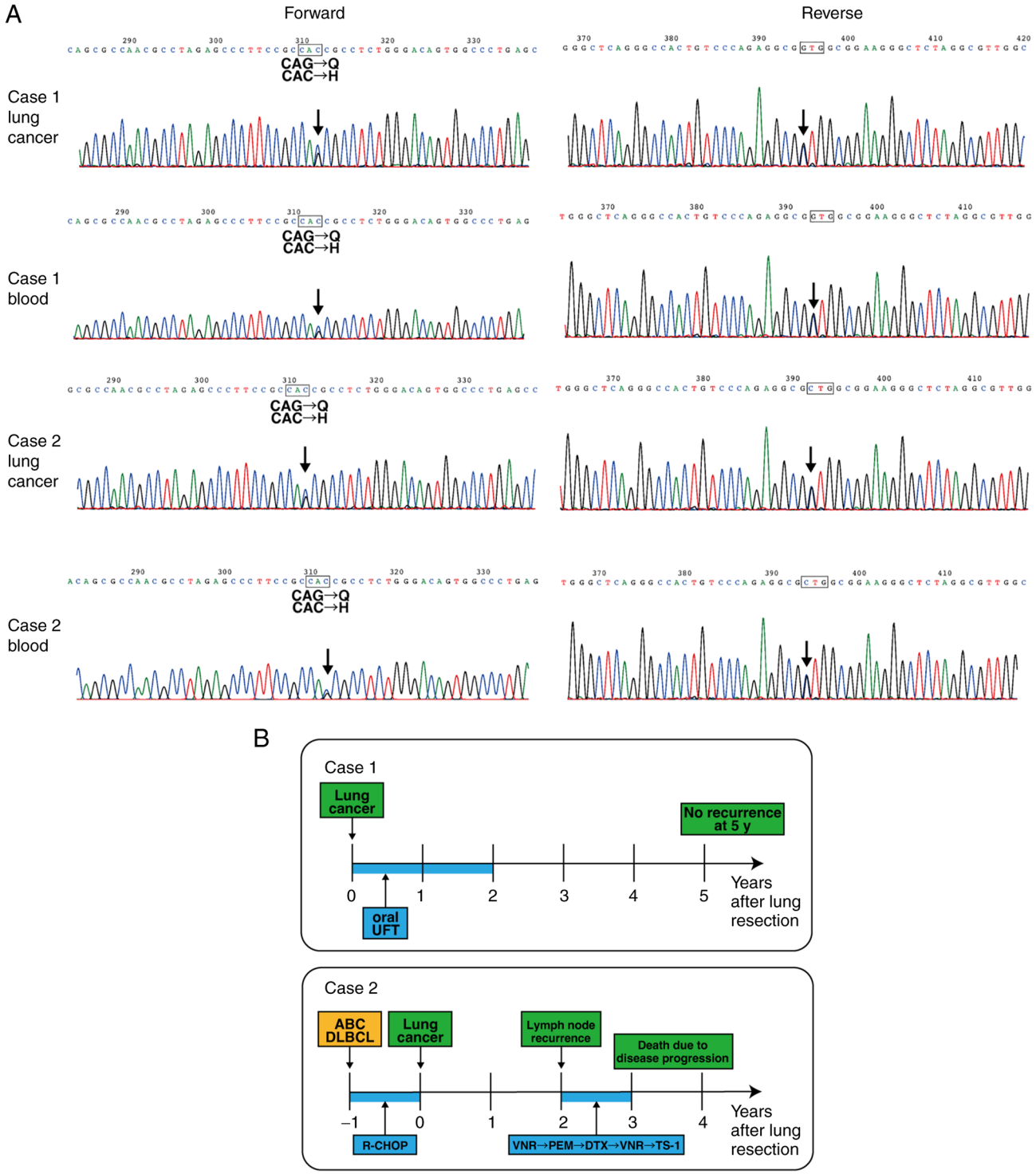

Figure 1. *RNF31* Q622H polymorphism in patients with lung cancer and ABC-DLBCL. (A) DNA sequence electropherograms of the region corresponding to the Q622H polymorphism in lung cancer and blood. (B) Clinical course of the patients with the Q622H polymorphism. UFT, uracil tegafur; ABC-DLBCL, activated B cell-like subtype of diffuse large B-cell lymphoma; R-CHOP, rituximab, cyclophosphamide, doxorubicin, vincristine, prednisone; VNR, vinorelbine; PEM, pemetrexed; DTX, docetaxel; TS-1, tegafur/gimeracil/oteracil; RNF31, RING finger protein 31.

Mutational status of lung cancer and ABC-DLBCL. Next, we examined co-mutations in the lung cancer and ABC-DLBCL specimens by cancer panel analysis. Fifteen variants were selected as candidate mutations. All samples harbored an *MSH2* mutation (Fig. 3, Table SII) with similar variant allele frequencies (0.59, 0.51, and 0.55 for lung cancer, ABC-DLBCL, and normal lung, respectively). We also detected *ARID1A*, *KMT2A*, *BRCA2*, *NFKBIA*, and *EP300* mutations common to all samples. The lung cancer sample was negative for *EGFR*, *KRAS*, *BRAF*, and *NRAS* mutations, but we detected mutations in *TP53*, *MET*, and *MTOR* that were not detected in the ABC-DLBCL lesion. In contrast, the ABC-DLBCL lesion harbored multiple mutations, including *B2M*, *FBXW7*, *CCND3*, *PIK3R1*, *PRDM1*, and *TNFAIP3* mutations.

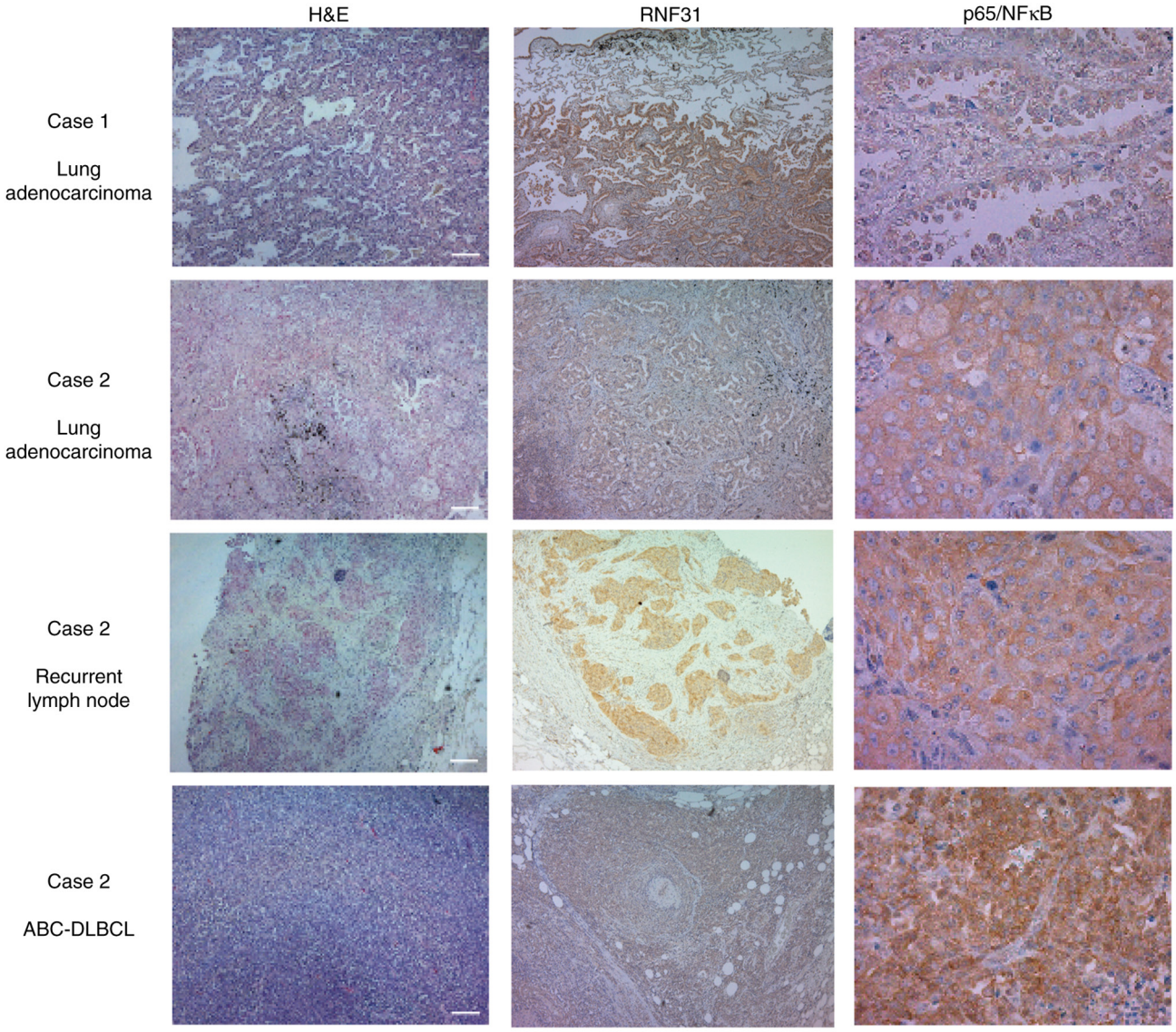

Figure 2. Histological findings of lung cancer and ABC-DLBCL with the *RNF31* Q622H polymorphism. HE staining and IHC of RNF31 and p65. HE staining showed well differentiated adenocarcinoma with lepidic growth for the lung cancer specimen (case 1); lung adenocarcinoma with solid component for the lung cancer, tumor cells surrounded with fibrous tissue for the lymph node recurrence, and large, atypical cells with high nuclear-cytoplasmic ratio for the ABC-DLBCL specimen (case 2). Scale bar for HE staining=200 μm, IHC images for p65 staining are magnified (x400) to clarify nuclear localization. HE, hematoxylin and eosin; IHC, immunohistochemistry; ABC-DLBCL, activated B-cell-like subtype of diffuse large B-cell lymphoma; RNF31, RING finger protein 31.

In vitro analysis of RNF31 Q622H. We next investigated the effect of *RNF31* Q622H on NF-κB activation, M1-Ub chain formation, and LUBAC complex formation. We compared the NF-κB activation induced by co-expression of RNF31 Q622H with RBCK1 and SHARPIN, in comparison to RNF31 Q584H and Q622L. When wild-type RNF31 and each mutant were over-expressed in 293T cells (Fig. 4A, lower panel), elevated NF-κB activation was detected in samples with RNF31 Q584H and Q622L mutants, in contrast to RNF31 Q622H, which showed no difference with wild-type RNF31 (Fig. 4A, upper panel). We then compared the formation of linear ubiquitin chains. In contrast to NF-κB activation, the level of M1-Ub formation was similar amongst all RNF31 mutants, with no significant increase in RNF31 Q584H and Q622L mutants (Fig. 4B). We also compared the binding ability of RNF31 mutants with RBCK1 and SHARPIN by co-immunoprecipitation but found no significant difference between RNF31 wild-type and RNF31 mutants (Fig. 4C).

Structural prediction of RNF31 Q622H. We further analyzed the effect of RNF31 Q622H on RNF31 and RBCK1 binding using the data from deposited crystal structures of RNF31 (Fig. 4) (18,19). We hypothesized that *RNF31* Q622H polymorphism could do one of the following: (1) directly affect the RNF31-RBCK1 interface; or (2) indirectly affect RNF31-RBCK1 binding by changing high-layer structures, i.e., *RNF31* Q622L polymorphism, which was proposed to affect the electrostatic interaction between RNF31 Q622 and E618 residues (10). In the crystal structures of human RNF31-RBCK1 and murine RNF31-RBCK1-SHARPIN complexes, the Q622 residue (or Q616 in mouse) is located in the ubiquitin-associated (UBA) domain of RNF31, which

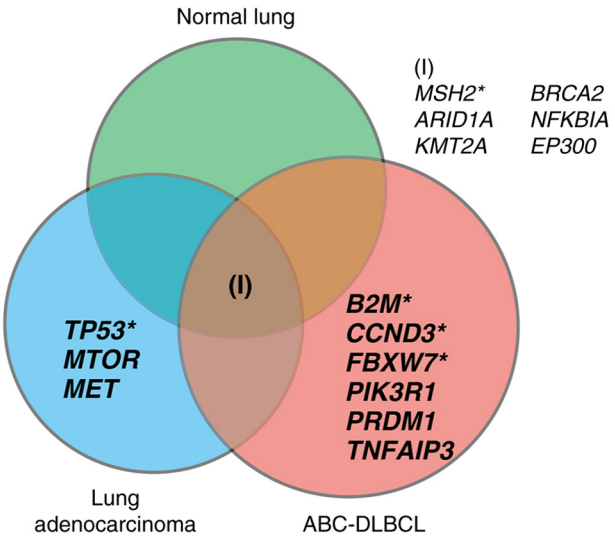

Figure 3. Genetic analysis of lung cancer and ABC-DLBCL in a patient with the *RNF31* Q622H polymorphism. Mutations detected in lung adenocarcinoma, ABC-DLBCL and adjacent normal lung tissue. Mutations identified by COSMIC v.70 selection are indicated with an asterisk. ABC-DLBCL, activated B-cell-like subtype of diffuse large B-cell lymphoma; RNF31, RING finger protein 31.

interacts with the ubiquitin-like (UBL) domain of RBCK1, leading to LUBAC formation (Fig. 4D and E). However, the side chain of the Q622 residue (Q616 in mouse) pointed towards the outside of the molecule and not the binding cleft between RNF31 and RBCK1. Therefore, the change in the Q622 residue might not directly affect RNF31- RBCK1 binding. Next, to compare the conformation of Q622 in the human and murine RNF31 structures, the Cα atoms of the C-terminal helix of the human RNF31 UBA (residues 610-624) in RNF31-RBCK1 was superposed onto the equivalent region of murine RNF31-RBCK1-SHARPIN with a root-mean-square deviation value of 0.857 (15 residues in total) (Fig. 4F). Superposition of the two structures showed that the human RNF31 Q622 formed an electrostatic interaction with E618, whereas the side chain of murine RNF31 Q616 and E612 pointed towards different directions (Fig. 4F). This suggests that the electrostatic interaction between murine E612 and Q616 (human E618 and Q622), which was previously proposed to affect the binding affinity between RNF31 and RBCK1 (10), is not a crucial interaction in the conformation of RNF31, at least in mice. Because this area is a highly conserved region of RNF31 amongst species, we speculated that the previously suggested human RNF31 E618 and Q622 electrostatic interaction is not crucial in humans either.

Discussion

Two germline polymorphisms of *RNF31* were previously reported as causative of ABC-DLBCL via enhanced binding between RNF31 and RBCK1, resulting in elevated NF-κB activation (10). Because NF-κB is involved in the carcinogenesis of various tumors (20), we searched for these NF-κB activating *RNF31* polymorphisms in lung cancer. Although no patient examined had the *RNF31* Q584H and Q622L polymorphisms, we identified a novel Q622H germline polymorphism in two patients with lung cancer, one of whom also had a history of ABC-DLBCL. Interestingly, although we detected strong expression of RNF31 in both lung cancer and ABC-DLBCL, NF-κB activation was only detected in the ABC-DLBCL specimen, suggesting that RNF31 Q622H was not an activator of NF-κB in these two cases of lung adenocarcinoma. Furthermore, *in vitro* analysis did not show enhanced binding between RNF31 Q622H and RBCK1, nor enhanced NF-κB activation or M1-Ub formation by Q622H, in comparison to RNF31 wild-type. Curiously, structural prediction failed to explain the role of Q622 in the binding between RNF31 and RBCK1 because the Q622 residue was not directly involved in the interaction of both molecules. We speculated that the reinforced binding effect reported for the Q622L polymorphism might be caused by a change in the higher layer structure and stability (10). We conclude that in contrast to the *RNF31* Q584H/Q622L polymorphisms, the Q622H polymorphism does not show enhanced NF-κB activation, linear ubiquitin formation, and RNF31-RBCK1 binding in comparison to RNF31 wild-type.

Studies have previously reported the clinical features of patients with RNF31 and RBCK1 mutations (Table SIII) (21-24). Mechanistically, the RNF31 L72P mutation destabilized RNF31 and LUBAC expression, leading to impaired NF-κB activation (21). *RBCK1* Q185X and L41fsX7 mutations also cause impaired NF-κB activation (22). Therefore, *in vitro*, LUBAC deficiency commonly leads to decreased NF-κB activation. However, *in vivo*, a decrease in or deletion of LUBAC components results in worse inflammation and subsequent carcinogenesis. For example, the homozygous *RNF31* L72P missense mutation results in multiorgan autoinflammation, combined immunodeficiency, subclinical amylopectinosis, and systemic lymphangiectasia (21). Similarly, patients with *RBCK1* mutations also present immunodeficiency, autoinflammation, and amylopectinosis. Such phenomena are also seen in the murine liver, in which deletion of LUBAC causes increased inflammation, resulting in hepatocarcinogenesis (25). These results suggest that LUBAC is not a simple activator of NF-κB, but rather a molecular rheostat that precisely modulates immune response and prevents carcinogenesis (11-12). In line with these findings, the patient with lung cancer and ABC-DLBCL in this study also had interstitial lung disease and pancreatitis, suggesting that the *RNF31* Q622H polymorphism may have promoted the development of these inflammatory diseases.

Critical signaling components are frequently mutated in lymphoma and lung cancer. These alterations induce gain or loss of function, overexpression, or deletion of genes. Previous reports have shown that an increase in RNF31 expression itself was insufficient to induce lymphoma (12). However, augmented LUBAC activity overcomes cell death induced by DNA damage, thereby accelerating the accumulation of somatic mutations. Thus far, the high number and variety of mutations present in DLBCL make it difficult to pinpoint which genetic lesions are driving the disease (26). In this study, mutation selection led to six gene mutations in ABC-DLBCL, including a frameshift mutation of *TNFAIP3*, which is a suppressor of linear ubiquitin signaling and NF-κB activation. We detected none of the *MYD88*, *CARD11*, *CD79B*, and *CD79A* mutations that have been previously reported in

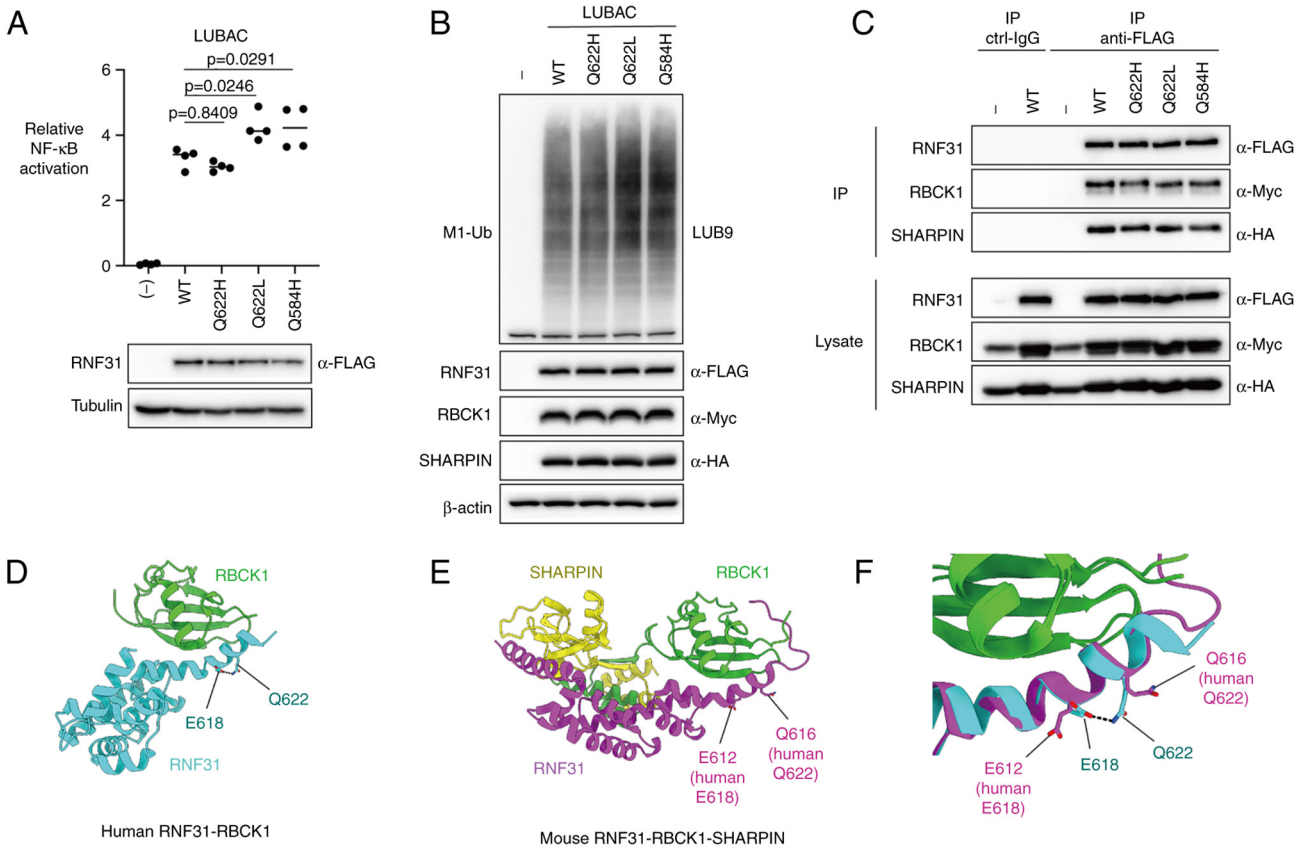

Figure 4. *In vitro* assessment and predicted crystal structure model of *RNF31* Q622H polymorphism. (A) Activation of NF-κB by RNF31 WT/Q622H/Q622L/Q584H. NF-κB activation by LUBAC was evaluated using luciferase reporter assay (upper panel) in *RNF31*-KO 293T cells. The expression of each protein was evaluated using western blotting (lower panel). (B) Linear ubiquitin formation by RNF31 WT/Q622H/Q622L/Q584H. The LUBAC expression vectors were co-expressed in *RNF31*-KO 293T cells, and cell lysates were immunoblotted with the indicated antibodies. (C) Effect of RNF31 Q622H/Q622L/Q584H polymorphisms on RNF31, RBCK1 and SHARPIN binding. FLAG-RNF31, RBCK1-myc, and HA-SHARPIN were overexpressed in *RNF31*-KO 293T cells, as indicated. The cell lysates and anti-FLAG immunoprecipitates were immunoblotted with the indicated antibodies. (D) Crystal structure of human RNF31 UBA domain (cyan) in complex with RBCK1 UBL domain (green) (PDB: 4dbg). (E) Mouse RNF31 UBA domain (magenta) in ternary complex with RBCK1 (green) and SHARPIN (yellow) (PDB: 5y3t). (F) Superposition of human and mouse RNF31 UBA domains. Interaction between human E618 and Q622 is shown in black dotted line. WT, wild-type; RNF31, RING finger protein 31; LUBAC, linear ubiquitin chain assembly complex; KO, knockout; RBCK1, RANBP2-type and C3HC4-type zinc finger containing 1; SHARPIN, SHANK-associated RH domain interactor; HA, hemagglutinin.

ABC-DLBCL patients with *RNF31* Q584H and Q622L polymorphisms (10). These findings suggest that although elevated NF-κB activation is a common feature of ABC-DLBCL, the underlying mutational background differs between patients with *RNF31* Q584H/Q622L vs. Q622H polymorphisms. Interestingly, mutations in the lung cancer specimen included *TP53* and *MTOR* mutations, as well as a *MET* mutation known to activate *MET* in a fashion similar to *MET* exon 14 skipping alterations (27,28).

A limitation of our study is that it was a retrospective study from a single institute. The cohort was therefore restricted to a Japanese population, and the prevalence of *RNF31* Q622H polymorphism was also low. A larger-scale analysis is necessary to further clarify the role of *RNF31* polymorphisms. Furthermore, our *in vitro* analysis of RNF31 was mainly conducted by overexpression and structural experiments. This might only depict one aspect of the *RNF31* polymorphism because its function might be cell line- or context-dependent.

To the best of our knowledge, this is the first study to analyze the *RNF31* Q584 and Q622 polymorphisms in lung cancer patients. The analysis revealed a previously unreported *RNF31* Q622H polymorphism in two patients with lung adenocarcinoma, one patient having concurrent ABC-DLBCL. We had speculated that *RNF31* Q622H could have molecular effects similar to Q584H and Q622L, which are *RNF31* polymorphisms causing ABC-DLBCL. However, RNF31 Q622H did not show enhanced LUBAC and NF-κB activation compared with the wild-type, nor enhanced RNF31-RBCK1-SHARPIN binding *in vitro*. The mutational background of *RNF31* Q622H ABC-DLBCL also differed from that of *RNF31* Q584H/Q622L ABC-DLBCL. Finally, there was a discrepancy between RNF31 expression and NF-κB activation in tumor specimen, suggesting that the involvement of the NF-κB pathway might be tissue-specific and the role of RNF31 could differ between lung cancer and ABC-DLBCL.

Acknowledgements

The authors would like to thank Dr Takayuki Kosaka (National Hospital Organization Takasaki General Medical Center, Takasaki, Japan) and Dr Ryosuke Kaneko (Osaka University, Suita, Japan) for expert advice; Dr Nobuhiko Kobayashi for

advice on ABC-DLBCL (Gunma University, Maebashi, Japan); Dr Kouki Hoshino, Ms Ayako Morita, Mr Hayato Kawabata, Mr Tatsuya Yamazaki, Mr Yohei Morishita, Ms Saori Umezawa, Ms Yoko Yokoyama, Ms Hiroko Matsuda, Dr Yuichi Uosaki and Mr Yusuke Goto for technical support (Gunma University, Maebashi, Japan).

Funding

This work was supported by KAKENHI Grant-in-Aid for Young Scientists B (grant nos. 17K14982 and 17K15038) and KAKENHI Grant-in-Aid for Young Scientists (grant no. 19K18203) Japan Society for the Promotion of Science, Takeda Science Foundation, and YOKOYAMA Foundation for Clinical Pharmacology (grant no. YRY-2006). This work was the result of using research equipment shared in the MEXT Project for promoting the public utilization of advanced research infrastructure, program for supporting the introduction of the new sharing system (grant no. JPMXS0420600120). This work was also supported by the Fostering Health Professionals for Changing Needs of Cancer by MEXT of Japan and Gunma University Initiative for Advanced Research (GIAR).

Availability of materials and data

The datasets generated during and/or analyzed during the current study are available from the corresponding author on reasonable request but are not publicly available due to the fact that the datasets have not been registered to a public database, in accordance to the study protocol.

Authors' contributions

SNa, DO and FT conceived and designed the study. SNa, RM, RKI, DO, KK, SNo, YS and AS acquired data. SNa, RM, RKI, DO, KK, FT, SNo, YS, AS, TY and KS made substantial contributions to data analysis and interpretation. SNa, RM, RKI, DO, KK, FT, SNo, YS, AS, TY and KS wrote, reviewed and/or revised the manuscript. SNa, DO, RKI, FT, KK, SNo, AS, TY and KS provided material support. SNa, RKI, FT, SNo, TY and KS supervised the study. SNa, DO and RKI confirm the authenticity of all the raw data. All authors read and approved the final manuscript.

Ethics approval and consent to participate

This study was approved by the ethics committee of Gunma University Faculty of Medicine (approval nos. 1344 and HS2021-219). Because of the retrospective design of the study, the requirement for written informed consent from each patient was waived.

Patient consent for publication

Not applicable.

Competing interests

The authors declare that they have no competing interests.

References

1. Yau R and Rape M: The increasing complexity of the ubiquitin code. Nat Cell Biol 18: 579-586, 2016.
2. Swatek KN and Komander D: Ubiquitin modifications. Cell Res 26: 399-422, 2016.
3. Grumati P and Dikic I: Ubiquitin signaling and autophagy. J Biol Chem 293: 5404-5413, 2018.
4. Popovic D, Vucic D and Dikic I: Ubiquitination in disease pathogenesis and treatment. Nat Med 20: 1242-1253, 2014.
5. Sasaki Y, Sano S, Nakahara M, Murata S, Kometani K, Aiba Y, Sakamoto S, Watanabe Y, Tanaka K, Kurosaki T and Iwai K: Defective immune responses in mice lacking LUBAC-mediated linear ubiquitination in B cells. EMBO J 32: 2463-2476, 2013.
6. Teh CE, Lalaoui N, Jain R, Policheni AN, Heinlein M, Alvarez-Diaz S, Sheridan JM, Rieser E, Deuser S, Darding M, *et al*: Linear ubiquitin chain assembly complex coordinates late thymic T-cell differentiation and regulatory T-cell homeostasis. Nat Commun 7: 13353, 2016.
7. Redecke V, Chaturvedi V, Kuriakose J and Häcker H: SHARPIN controls the development of regulatory T cells. Immunology 148: 216-226, 2016.
8. Klein T, Fung SY, Renner F, Blank MA, Dufour A, Kang S, Bolger-Munro M, Scurll JM, Priatel JJ, Schweigler P, *et al*: The paracaspase MALT1 cleaves HOIL1 reducing linear ubiquitination by LUBAC to dampen lymphocyte NF-κB signalling. Nat Commun 6: 8777, 2015.
9. Song Z, Wei W, Xiao W, Al-Saleem ED, Nejati R, Chen L, Yin J, Fabrizio J, Petrus MN, Waldmann TA and Yang Y: Essential role of the linear ubiquitin chain assembly complex and TAK1 kinase in A20 mutant Hodgkin lymphoma. Proc Natl Acad Sci USA 117: 28980-28991, 2020.
10. Yang Y, Schmitz R, Mitala J, Whiting A, Xiao W, Ceribelli M, Wright GW, Zhao H, Yang Y, Xu W, *et al*: Essential role of the linear ubiquitin chain assembly complex in lymphoma revealed by rare germline polymorphisms. Cancer Discov 4: 480-493, 2014.
11. Dubois SM, Alexia C, Wu Y, Leclair HM, Leveau C, Schol E, Fest T, Tarte K, Chen ZJ, Gavard J and Bidère N: A catalytic-independent role for the LUBAC in NF-κB activation upon antigen receptor engagement and in lymphoma cells. Blood 123: 2199-2203, 2014.
12. Jo T, Nishikori M, Kogure Y, Arima H, Sasaki K, Sasaki Y, Nakagawa T, Iwai F, Momose S, Shiraishi A, *et al*: LUBAC accelerates B-cell lymphomagenesis by conferring resistance to genotoxic stress on B cells. Blood 136: 684-697, 2020.
13. Yokobori T, Bao P, Fukuchi M, Altan B, Ozawa D, Rokudai S, Bai T, Kumakura Y, Honjo H, Hara K, *et al*: Nuclear PROX1 is associated with hypoxia-inducible factor 1α expression and cancer progression in esophageal squamous cell carcinoma. Ann Surg Oncol 22 (Suppl 3): S1566-S1573, 2015.
14. Sasaki A, Hirato J, Hirose T, Fukuoka K, Kanemura Y, Hashimoto N, Kodama Y, Ichimura K, Sakamoto H and Nishikawa R: Review of ependymomas: Assessment of consensus in pathological diagnosis and correlations with genetic profiles and outcome. Brain Tumor Pathol 36: 92-101, 2019.
15. Tate JG, Bamford S, Jubb HC, Sondka Z, Beare DM, Bindal N, Boutselakis H, Cole CG, Creatore C, Dawson E, *et al*: COSMIC: The catalogue of somatic mutations in cancer. Nucleic Acids Res 47 (D1): D941-D947, 2019.
16. Tokunaga F, Nakagawa T, Nakahara M, Saeki Y, Taniguchi M, Sakata S, Tanaka K, Nakano H and Iwai K: SHARPIN is a component of the NF-κB-activating linear ubiquitin chain assembly complex. Nature 471: 633-636, 2011.
17. Tokunaga F, Sakata SI, Saeki Y, Satomi Y, Kirisako T, Kamei K, Nakagawa T, Kato M, Murata S, Yamaoka S, *et al*: Involvement of linear polyubiquitylation of NEMO in NF-kappaB activation. Nat Cell Biol 11: 123-132, 2009.
18. Fujita H, Tokunaga A, Shimizu S, Whiting AL, Aguilar-Alonso F, Takagi K, Walinda E, Sasaki Y, Shimokawa T, Mizushima T, *et al*: Cooperative domain formation by homologous motifs in HOIL-1L and SHARPIN plays A crucial role in LUBAC stabilization. Cell Rep 23: 1192-1204, 2018.
19. Yagi H, Ishimoto K, Hiromoto T, Fujita H, Mizushima T, Uekusa Y, Yagi-Utsumi M, Kurimoto E, Noda M, Uchiyama S, *et al*: A non-canonical UBA-UBL interaction forms the linear-ubiquitin-chain assembly complex. EMBO Rep 13: 462-468, 2012.
20. Karin M: NF-kappaB as a critical link between inflammation and cancer. Cold Spring Harb Perspect Biol 1: a000141, 2009.

21. Boisson B, Laplantine E, Dobbs K, Cobat A, Tarantino N, Hazen M, Lidov HG, Hopkins G, Du L, Belkadi A, *et al*: Human HOIP and LUBAC deficiency underlies autoinflammation, immunodeficiency, amylopectinosis, and lymphangiectasia. J Exp Med 212: 939-951, 2015.
22. Boisson B, Laplantine E, Prando C, Giliani S, Israelsson E, Xu Z, Abhyankar A, Israël L, Trevejo-Nunez G, Bogunovic D, *et al*: Immunodeficiency, autoinflammation and amylopectinosis in humans with inherited HOIL-1 and LUBAC deficiency. Nat Immunol 13: 1178-1186, 2012.
23. Nilsson J, Schoser B, Laforet P, Kalev O, Lindberg C, Romero NB, Dávila López M, Akman HO, Wahbi K, Iglseder S, *et al*: Polyglucosan body myopathy caused by defective ubiquitin ligase RBCK1. Ann Neurol 74: 914-919, 2013.
24. Oda H, Beck DB, Kuehn HS, Sampaio Moura N, Hoffmann P, Ibarra M, Stoddard J, Tsai WL, Gutierrez-Cruz G, Gadina M, *et al*: Second case of HOIP deficiency expands clinical features and defines inflammatory transcriptome regulated by LUBAC. Front Immunol 10: 479, 2019.
25. Shimizu Y, Peltzer N, Sevko A, Lafont E, Sarr A, Draberova H and Walczak H: The linear ubiquitin chain assembly complex acts as a liver tumor suppressor and inhibits hepatocyte apoptosis and hepatitis. Hepatology 65: 1963-1978, 2017.
26. Pomerantz JL: HOIP for targeting diffuse large B-cell lymphoma. Blood 136: 646-647, 2020.
27. Awad MM, Oxnard GR, Jackman DM, Savukoski DO, Hall D, Shivdasani P, Heng JC, Dahlberg SE, Jänne PA, Verma S, *et al*: MET exon 14 mutations in non-small-cell lung cancer are associated with advanced age and stage-dependent MET genomic amplification and c-Met overexpression. J Clin Oncol 34: 721-730, 2016.
28. Frampton GM, Ali SM, Rosenzweig M, Chmielecki J, Lu X, Bauer TM, Akimov M, Bufill JA, Lee C, Jentz D, *et al*: Activation of MET via diverse exon 14 splicing alterations occurs in multiple tumor types and confers clinical sensitivity to MET inhibitors. Cancer Discov 5: 850-859, 2015.